This document is the Accepted Manuscript version of a Published Work that appeared in final form in APPLIED SURFACE SCIENCE, copyright © Elsevier Ltd after peer review and technical editing by the publisher. To access the final edited and published work see [https://doi.org/10.1016/j.apsusc.2020.146443]
Licence CC BY-NC-ND

Graphene as non conventional transparent conductive electrode in silicon heterojunction solar cells

Laura Lancellotti*, Eugenia Bobeico, Marco Della Noce, Lucia V. Mercaldo, Iurie Usatii, Paola Delli Veneri

Italian National Agency for New Technologies, Energy and Sustainable Economic Development (ENEA) – Portici Research Centre, Piazzale E. Fermi 1, 80055 Portici (Na), Italy

Giuseppe Valerio Bianco, Alberto Sacchetti, Giovanni Bruno

CNR-NANOTEC Institute of Nanotechnology, Apulian Graphene Lab, Department of Chemistry, University of Bari, via Orabona 4, Bari, 70126, Italy

Abstract

Chemical Vapor Deposited (CVD) graphene is an attractive candidate as transparent conductive electrode (TCE) for solar cells. Here it is proposed as TCE for silicon heterojunction solar cells (Si-HJSCs) and tested over devices with area up to 4 cm^2 realized on n-type c-Si wafers with three different p-type emitters facing the dry-transferred graphene stack: amorphous silicon (a-Si:H), nanocrystalline silicon (nc-Si:H), and nanocrystalline silicon oxide (nc-SiO_x:H). A dependence of the cell performance on the material in contact with graphene has been observed with the most promising results in case of nc-Si:H and nc-SiO_x emitter. In particular, with respect to reference cells with standard TCE a short circuit current density gain of 1.4 mA/cm^2 has been achieved when including an antireflection coating. The present work demonstrates the high quality of dry-transferred CVD-graphene over relatively large area and the feasibility of Si-HJSCs integrating graphene, where the fabrication sequence asks for a transfer process that guarantees a much better contact with the underlying functional layer with respect to more common designs where graphene is transferred onto a support substrate. This approach provides a possible pathway to Si-HJSCs free from conventional plasma-based TCEs and their deleterious effects due to plasma luminescence and ion bombardment, while offering an interesting platform for getting insights in the mechanisms at play at the interfaces with graphene within Si wafer-based devices.

Keywords:graphene, heterojunction, solar cells

*Corresponding author. Tel: 0039-0817723245. E-mail: laura.lancellotti@enea.it

1. Introduction

The unique electrical, optical, mechanical and optoelectronic properties of graphene have attracted great attention and opened up an enormous number of opportunities in different research areas. Among these, a lot of scientific research is being carried out in the solar cell field, where graphene can function as electrode and/or active layer for electron–hole separation and hole transport. Core issues in graphene-integrated solar cells are outlined in many papers and review articles [1-5].

The limitations in growing and transferring graphene are among the major obstacles in the progress of graphene-integrated devices where the large area is relevant (> 0.2 cm^2). This challenge is prominent for photovoltaic devices because a large area is there required for proper solar energy harvesting. The R&D activities to realize cost-efficient synthesis of highly crystalline graphene are however progressing fast and several notable results have already been reported at mass production scale for large area graphene [3], although the question is still open even at laboratory scale [6-9]. Among the most promising approaches, Chemical Vapour Deposition (CVD) technology allows the synthesis of high-quality large-area graphene in controlled and reproducible way. Thanks to the improvement of transfer methods, CVD-graphene may prove viable for a variety of large area applications. In particular, it has been successfully employed as transparent electrode within organic photovoltaic (OPV) devices and dye sensitized solar cells [10, 11].

In the present work, for the first time to our knowledge, we investigate the feasibility of CVD-graphene as TCE for silicon heterojunction solar cells (Si-HJSCs). In recent years, this photovoltaic technology has demonstrated energy conversion efficiencies well above 25%, thus proving to be a very effective approach for high efficiency photovoltaics [12, 13]. The most common cell architecture is based on a crystalline silicon (c-Si) wafer with front and back surface passivated by ultrathin intrinsic hydrogenated amorphous silicon (a-Si:H) covered with p-type doped a-Si:H on one side and n-type doped a-Si:H on the opposite side, functioning as selective charge carrier collectors. For better use of the sunlight, the wafers are etched to form textured surfaces with random micron-scale pyramids, in order to gain from antireflection and light trapping effects. A transparent conductive electrode (TCE) is applied to the front side, with electrical and optical function (to cope with the insufficient lateral conduction in the thin film silicon doped layer and simultaneously provide antireflection effect), followed by a metal grid, while a full area metal electrode typically covers the

back side. The most common TCEs are sputtered indium tin oxide (ITO) and Al-doped ZnO (AZO) that require handling of issues caused by plasma luminescence and ion bombardment.

Based on its favorable electrical and optical properties, we here propose few-layer graphene as a plasma-free alternative to conventional TCEs within Si-HJSCs. The novelty of our work is twofold. Firstly, we extend the application of graphene to one of the most efficient photovoltaic technologies with a strong commercial potential. In addition, we explore and demonstrate the feasibility of an unconventional technological scheme. In most applications, CVD-graphene is indeed transferred onto the physical support where the device is afterwards fabricated, thus employing a device-over-graphene design [11, 14-16]. In the present work, the solar cell architecture requires instead an inverted graphene-over-device approach, where the transfer step on the underlying functional material is more delicate. In the more common case, the graphene stack has to adhere to an external substrate and intimate contact is not mandatory. In the inverted approach, formation of perfect contact with the underlying layer is required, as this interface is internal to the device.

We have synthesized CVD graphene with grain sizes up to 200 μm^2 and developed a layer-by-layer dry-transfer method to minimize chemical contamination. The transferred graphene stacks have been characterized from structural, optical and electrical point of view. The few-layer stacks with suitable properties (4- and 5- layer) have been then tested as front TCE in flat n-type Si-HJSCs with active area up to 4 cm^2. We have here selected flat Si wafers as a more defined experimental setting at the present proof-of-concept stage of the graphene-over-device approach, due to the additional complication arising with the transfer over a textured surface. Even with flat surfaces the success of the transfer process is not obvious, as many factors can influence the adhesion. We have thus devised to test the process over solar cells with different emitters (the upmost layer prior to graphene), investigating in particular three p-type doped thin film Si-based layers: amorphous silicon (a-Si:H), nanocrystalline silicon (nc-Si:H) and nanocrystalline silicon oxide (nc-SiO_x:H). In the first place, we have gained insight into various mechanisms at play at the interfaces with graphene within the sequence metal/graphene/p-type-emitter/n-type-Si-wafer. Regarding the potential of the novel device, in most cases we have obtained functioning solar cells. We have observed a dependence on the emitter material, with promising results in case of nc-Si:H and nc-SiO_x. Finally, with the application of a double antireflection coating (DARC) we have revealed a potential gain in short circuit current density.

2. Experimental section

Graphene was synthesized by chemical vapor deposition (CVD) on copper foils (Sigma Aldrich 349 208, 25 mm thick) at 1000 ^{0}C with CH_4:H_2 as precursors and a total pressure of 0.3 Torr. Single layer and few layer graphene foils were firstly transferred onto appropriate substrates for material characterization (Corning glass substrates and n-type Si wafers) by thermal tape methodology dissolving copper in a solution of ammonium persulfate (2% APS).

For solar cells fabrication, we used flat n-type float-zone c-Si<100> wafers with resistivity of 1–5 Ω cm and thickness of 270 μm. The full structure of the device is schematized in Fig. 1. Before starting the fabrication sequence, the wafers were cleaned with the RCA procedure and dipped in 2% HF to remove the native oxide. The wafers were then passivated on both sides with an intrinsic a-Si:H layer with thickness of ~ 5 nm. The back side of the solar cells was completed with n-type SiO_x layers (20 nm), functioning as back surface field, followed by a full area contact made of 80-nm-thick AZO layer plus Al. On the front side, different emitters were considered, namely p-type doped layers of a-Si:H (10 nm), nc-Si:H (20 nm), and nc-SiO_x (20 nm). The Si- and SiO_x- based layers were grown by Plasma Enhanced Chemical Vapor Deposition (PECVD) in an MVSystems Inc. cluster tool system. Details of the deposition apparatus and of the experimental fabrication conditions are reported elsewhere [17-19]. AZO layers were deposited by RF sputtering at 13.56 MHz with Ar plasma and no intentional substrate heating in a MRC system starting from a doped ZnO target (2 wt% Al_2O_3). After AZO deposition, a thermal treatment was usually applied (180 °C for 30 min in vacuum).

Graphene was transferred on top of the emitter of the solar cells with a multi-step procedure (layer by layer) using the thermal release tape transfer: the tape with graphene was pressed onto the solar cell surface with a rubber roll and, when heated at 100°C, the graphene layer detached and transferred to the underlying surface. Reference cells were also fabricated, with 80 nm thick sputtered AZO as antireflective TCE. All the solar cells, with active areas of 1x1cm^2 or 2x2cm^2, were completed with a front 5 μm-thick Al collection grid. Finally, for selected solar cells with graphene, a double antireflection coating (DARC), made of 51.5nm of ZnS followed by 100.6nm of MgF_2, was thermally evaporated on top of the front metal grid.

Graphene films were electrically and optically characterized. UV–Vis–NIR transmittance spectra were measured with a Perkin Elmer Lambda 900 spectrometer. The sheet resistance of the films was determined through a four-point probe technique using Keithley 2400 source meter. For structural characterization Raman spectra were measured with a Horiba Jobin-Yvone HR-spectrometer using a 532 nm wavelength laser. Work function (WF) maps were obtained through the Kelvin probe technique using an SKP5050 instrument of KP Technology [20, 21].

Unfinished solar cells (at various stages prior to metallization) were characterized by means of photoconductance decay technique using a Sinton WCT-120 lifetime tester in transient mode. The

solar cells were characterized by measuring dark and illuminated current-voltage characteristics and external quantum efficiency (EQE). Dark I(V) curves were measured with a Keithley 236 electrometer. The illuminated J-V curves were evaluated under AM1.5G spectrum with a WACOM class AAA dual-lamp solar simulator using a shadow mask aligned to the cell area. The EQE was measured with a Bentham PVE300 setup with white light bias close to 1-sun intensity.

3. Results and discussion

3.1 Graphene characterization

The quality of the single layer graphene samples, in terms of grain sizes, presence of multilayer islands, wrinkles, folds or cracks, has been evaluated by optical microscope images (before and after transfer on glass substrates) and by Raman mapping. Fig. 2(A) shows the optical image of graphene/Cu after selective oxidation of the underlying copper foil, through graphene grain boundaries with oxygen under wet conditions and ambient light irradiation. The lines of oxidized copper become visible, thereby allowing the visualization of the graphene grain boundaries. The estimated average area of the graphene flakes is 100÷300 mm^2. The optical image of the single layer graphene after the transfer on Corning glass is shown in Fig. 2(B). The image contains areas that differ in graphene thickness. The small lighter regions have two graphene layers. The second graphene layer nucleates below the single layer forming an inverted wedding cake (IWC) [22]. The Raman characterization results are shown in Figs. 2(C) and 2(D). The map in panel (C) is based upon the typical G-band at 1580 cm^{-1} and 2D-band at 2672cm^{-1}, and in particular upon the 2D/G intensity ratio by using a color scale, with red representing monolayer graphene and blue representing bilayer graphene (IWC). Representative Raman spectra of monolayer (red) and bilayer (blue) regions are shown in panel (D).

Raman characterization was repeated also for graphene transferred onto the solar cells. The spectra of 1-, 4- and 5-layers graphene foils, are shown in Fig. 3. The almost complete absence of the D-band at 1350 cm^{-1} is indication of good quality material, since this band appears as long as the contribution from defects, mainly sp^3-C, increases. When moving from the 1L to the 4L and 5L stacks, the intensity of the G and 2D peaks increases by almost 4 and 5 times, respectively. At the same time, the I_{2D}/I_G ratio, the parameter normally used to estimate the number of layers, is >2, typical for single-layer graphene. These results suggest the formation of a twisted multilayer structure, because in this case the ratio does not change significantly as the number of layers increases [23-25].

The graphene stacks have been further characterized in view of the proposed application. The properties required to a material to be applied as TCE are low sheet resistance, high optical

transmittance, low reflectance and workfunction matched to the underlying layer. Starting with the optical properties, Fig. 4 shows the transmittance spectra of the graphene films with different nL transferred onto glass substrates compared with the transmittance of AZO layers with thickness of 20, 40, and 80 nm deposited on the glass. The transmittance gradually decreases with the number of layers on the whole visible spectral range, going from 97.5% at 550 nm for 1L to 91% and 88.5% for 4L and 5L samples, respectively. Still, even for the 5L sample the entire curve remains well above the transmittance spectrum of the 80 nm thick AZO layer on glass, which is the typical AZO thickness applied to the front side of Si HJSCs so that the layer simultaneously functions as TCE and antireflection coating. Even reducing the thickness by a factor 2, the transmittance of AZO remains below that of the 5L graphene stack. To reach this level, the AZO thickness has to be reduced down to 20 nm, which is unfeasible for application as TCE due to unsuitable electrical properties (Fig. 4).

Moving to the electrical properties, Fig. 5 shows the sheet resistance of the same graphene and AZO samples of Fig. 4. Values around 100 Ω/square are typically targeted for TCEs applied onto Si HJSCs, as it is for the 80 nm thick AZO sample (~170 Ω/square in the present case). When reducing the AZO thickness even by a factor of 2 only, the sheet resistance reaches ~500 Ω/square, while with the 20 nm thick sample, roughly an extra factor of 10 is gained, making such layers unsuitable as TCEs. Single layer graphene is also unsuitable (~750 Ω/square), while starting from the 3L stack and over, the sheet resistance of graphene gets close to and even lower than that of 80 nm thick AZO. The combined optical and electrical properties of Figs. 4 and 5 show the good potential of the graphene samples as superior TCE with respect to 80 nm thick AZO. As for the missing antireflection effect with graphene, a supplementary coating can be applied specifically tailored to maximize the antireflection effect and thus with possible additional gain with respect to the single multifunction AZO layer.

Another important issue is the energy band alignment of the TCE with the underlying layer in the solar cells. When considering the p-layer/i-a-Si:H/n-c-Si junction, the thin film p-layer/i-a-Si stack acts as a passivating hole selective contact by providing chemical passivation plus a built-in electric field that repels electrons from the interface or, in other terms, a band bending leading to an inversion layer inside the n-type c-Si wafer close to the interface. When applying a TCE overlayer, a negatively mismatched WF would have a detrimental impact on the band bending and thus on the selectivity of the hole contact. An opposing diode may form which can strongly influence the device performance, at an extent that depends also on doping level and thickness of the p-type layer contacted by the TCE (i.e. on the ability of the p-type layer to screen the opposing band banding originated by the TCE) [17, 26]. On this basis, a TCE with high WF is desired on the p-layer to avoid detrimental distortions of the current-voltage characteristics of the solar cell. The relevant parameter would be

the effective ΔWF at the internal interface within the device, which likely differs from the estimate based on measurements of dedicated samples. Although not significant in its absolute value, the measured WF can still allow for comparative trends when changing the TCE applied to the emitter. As for the p-type emitter layers in the solar cell, the WF is given by ($\chi + E_g - E_a$), where χ, E_g, and E_a are electron affinity, bandgap, and activation energy, respectively, making for values above 5 eV in all the relevant cases. A sub-optimal WF of 4.4 eV has been evaluated for 80 nm thick AZO, the TCE of the reference solar cells, while graphene may prove to be more favorable. First of all, it has been reported that on p-type silicon graphene tends to form ohmic or low-barrier contact, due to unintentional p-doping caused by air exposure and transfer process [4, 27]. In our case, where few layer graphene is applied, for comparison purpose we have estimated the WF of a 5L stack to benefit from the fact that graphene WF increases with the number of layers [28]. The measured map of 5L graphene transferred on Si is shown in Fig. 6 and the calculated mean value of the WF on the scanned area is 4.65 eV. Based on the measured values, when replacing AZO with 5L graphene we can in principle expect a more favorable WF mismatch with the underlying p-type layer, and then a lower junction barrier. We will further discuss WF effects in Section 3.3 when commenting on lifetime characterization of unfinished solar cells (prior to metallization) and on full device performance, where the effect of the metal is included.

3.2 Proof of concept on 1 cm^2 solar cells

Growing and transferring high-quality large-area graphene, especially over a functional layer within a device is not a straightforward task. As a first attempt, we have thus tested relatively small area solar cells (1 cm^2): 4L and 5L graphene films have been transferred onto nominally identical Si-HJSCs with p-type doped nc-Si:H emitter. The illuminated current–voltage characteristics of the solar cells are shown in Fig. 7 and the corresponding photovoltaic parameters are reported in Table I. Data for the reference solar cell using 80 nm thick AZO as TCE are also reported for comparison. All the cells with graphene are operational, with very similar values among the cells for each photovoltaic parameter and slightly better performance in case of 5L graphene. The short circuit current density is impacted by the missing antireflection effect, thus explaining the large difference versus the solar cell with AZO (up to 7.2 mA/cm^2). Also the other photovoltaic parameters (V_{oc} and FF) are currently inferior with respect to the reference cell. However, good repeatability is observed within each set of cells. In addition, the dark I(V) characteristics show superior response of the graphene integrating cells with respect to the reference cell (Fig. 8), with a low reverse current (leakage current) and a high rectifying ratio at V=±1V (~ 10^4), indicating a good passivation level and a low shunt effect. Well

preserved passivation and better shunt resistance are likely beneficial effects of the soft graphene transfer process, against the aggressive sputtering method for AZO deposition.

In order to evaluate the potential gain of short circuit current when using graphene as TCE, we have applied a double antireflection coating (DARC) on the front side of the graphene integrating cells by thermal evaporation of ZnS and MgF_2. The thickness of the two components of the DARC coating was optimized by means of Essential Macleod software [29]. The compatibility of graphene with the deposition of the DARC has been already shown [30, 31]. The EQE of the best solar cell with graphene plus DARC is compared in Fig. 9 with the EQE of the reference cell with AZO. A gain is observed with graphene, corresponding to an increase of the short circuit current density of 1.4 mA/cm^2.

3.3 Solar cells with different emitters

To investigate the potential of graphene integrated Si-HJSCs, we designed a second experiment where the graphene stack is applied onto different p-type doped materials used as emitter in the Si HJSC structure. Both fully amorphous and mixed-phase nanocrystalline materials, Si-based and SiO_x-based, can be applied as charge collectors in Si-HJSCs [17-19, 32-34], opening for a rather broad variation of the emitter/TCE interface conditions in terms of morphology, WF, etc. We tested three p-type layers, previously optimized for use within thin film silicon solar cells and Si-HJSCs [17-19]: a-Si:H, nc-Si:H, nc-SiO_x:H, where the latter two materials feature a Si nanocrystal phase in an amorphous silicon or amorphous silicon oxide background tissue, respectively. As for the graphene stack, the present test was limited to the 5L only, based on the better performance observed among the 1 cm^2 solar cells of the first test. In addition, larger area devices (4 cm^2) were fabricated in this second experiment to simultaneously test the feasibility of the approach when scaled over an enlarged area.

Firstly, a lifetime investigation was carried out on solar cell precursors (unfinished solar cell structures prior to the deposition of metal electrodes) as a means to evaluate the interaction between the graphene foil and the underlying emitter in terms of Si wafer passivation. In Fig. 10 the injection dependent effective minority carrier lifetime of the structures prior to the application of any frontal TCE, is compared with the same structures after the deposition of AZO or transfer of 5L graphene on the front side for the three different emitters.

The starting lifetime curve is similar with all the emitters, indicating comparable passivation level achieved in all the cases. After the application of the AZO capping layer (reference TCE) and

subsequent annealing, no shift along the y-axis but strong modification of the curve shape is observed for all the structures with significant decrease at low injection. The absence of vertical shift of the curve indicates no relevant variation of the chemical passivation. This is because, although plasma-based deposition methods have detrimental effect on the passivation due to plasma luminescence and possibly also ion bombardment, thermal annealing usually allows to recover the original condition [17, 35-37]. On the other hand, thermal annealing has no effect on the lifetime decay at low injection, which is most likely due to the mere presence of the AZO overlayer with its energy band misalignment with the underlying p layers causing a reduction of the so-called field effect passivation mechanism, i.e. a suppression of the band bending in the wafer [17, 38-40]. With a WF of 4.4 eV for AZO, a band misalignment is expected with all the emitters under test, as anticipated in Section 3.1. This means that depletion likely occurs in the p-type doped layers eventually reducing the built-in electric field at the interface with the Si wafer that repels electrons (field effect passivation). We cannot exclude a concurrent deterioration of the p-type layers because of ion bombardment during the AZO deposition by sputtering.

As for the same cell structures completed with the 5L graphene stack, the lifetime remains essentially unchanged over the whole range. The absence of any significant vertical shift of the curve is proof that the chemical passivation remains the same after the graphene transfer process. In addition, the unaltered shape at low injection might indicate a more favorable band alignment with the underlying p-type layers (in agreement with the the WF discussion reported in section 3.1), and/or the absence of possible plasma-related deterioration of the p-layer thanks to a plasma-free approach for TCE deposition. On the other hand, the absence of lifetime curve modification after graphene integration may also come from a weak electrical interaction between graphene and the underlying layer, maybe because of a still not perfect adhesion.

Representative J(V) curves under illumination of the complete devices after metallization are shown in Fig. 11. The corresponding electrical parameters are reported in Table II. Functioning solar cells with comparable characteristics have been obtained with the two nanocrystalline emitters, while the devices with p-a-Si:H emitter suffer from extremely poor performance.

Besides looking at the present efficiency of the devices, this second experiment with different p-type emitter materials allows to highlight interface issues of various nature. Focusing first on the graphene/emitter interface, the hindered carrier extraction may be caused by a variety of phenomena, going from surface morphology to material defect density, and to interfacial chemistry. Among the main effects, we speculate that the extraction of carriers might be hindered by a still not optimal adhesion of the graphene stack to the underlying functional layer. This problem could be emphasized in case of p-a-Si:H due to its totally flat surface, while being almost completely overcome with the

nanocrystalline materials characterized by a nanorough surface where the graphene foil can more easily anchor. Moreover, since a-Si:H has a higher defect density with respect to nc-SiO_x and nc-Si:H, an increased electronic scattering from surface defects may affect the mobility of carriers in the graphene transferred onto the a-Si:H emitter, with the consequence of a deteriorated performance of the corresponding device. Also nc-SiO_x and nc-Si:H are defective materials, although to a minor extent. Another contribution could be the different chemistry at the interface with graphene, linked to the different content of Si and O dangling bonds and hydrogen on the various p-type material surfaces. In particular, the interaction between hydrogen at the hydrogenated thin film emitter surface and the carbon π-plane may affect the bond structure of graphene [41] with effects on the band diagram and then on the device performance.

The front interface of graphene with the metal grid can also impact the device performance. In the case of the degenerately doped 80-nm-thick AZO layer, the capping metal grid is electrically fully screened from the hole-collecting interface. On the other hand, when using graphene as TCE, considering that the Fermi level at the Dirac point is easily shifted, the WF of the metal is a relevant parameter. In the present work, the low cost Al grid was maintained as in the standard reference solar cells. Graphene is likely unable to fully screen the low-WF Al electrode, possibly impacting the band bending in the wafer and thus the selectivity of the front contact. Such an effect is expected to be less severe when using an emitter layer with higher doping level (lower activation energy), which by itself can better shield a misaligned capping layer with beneficial effect on the band diagram and consequently on the cell performance. These considerations provide a possible additional and/or alternative explanation for the superior performance of the solar cells employing nanocrystalline emitters, characterized by larger conductivity and lower activation energy than the amorphous counterpart thanks to their higher doping efficiency [17,19]. It is however difficult to quantify the contribution of this effect because of the front electrode configuration with partial coverage of graphene by the Al grid (not full-area coverage), where only the graphene below the thin fingers interact with the metal. With this geometry, it has been shown that the impact on the graphene WF is strictly dependent on material and geometry of the metal grid [42]. Further experiments should be considered for testing different metals and designs of the frontal grid, while also taking into account wettability issues between metal and graphene and effects on contact resistance [43].

Commenting on the scale-up, in the present experiment the FF is slightly lower than in the 1 cm^2 cell batch. This is most likely an effect of the increased difficulty when scaling the application over a significantly enlarged area. Nevertheless, at this stage we have succeeded at demonstrating working graphene-integrated Si-HJSCs with area up to 4 cm^2. As future step we aim at progressing with solar cell efficiency by: 1)optimizing the upper contact grid through a careful selection of the type of metal

and proper modification of the grid geometry, and 2) setting up proper surface treatments prior to the transfer process in order to favor the adhesion of graphene.

In addition, an alternative methodology for direct transfer of multiple-layer graphene is under development to replace the current multi-step transfer process, as a technical simplification to meet the demands of the PV manufacturing industry.

4. Conclusions

CVD graphene has been synthesized and transferred onto different substrates and onto unfinished Si-HJSCs to be characterized and tested as innovative front transparent conductive electrode. The material characterization has shown that the devised layer-by-layer transfer method provides good quality material with twisted multilayer structure. As for electrical and optical properties, with five layers a sheet resistance of 100 Ω/square has been achieved while maintaining a relatively high transmittance (higher than 85% over the whole visible range). Si-HJSCs cells using n-type Si wafers have been fabricated and completed by transferring graphene on the front side of different p-type doped Si- and SiO_x-based emitters. While the graphene integration with p-a-Si:H emitter is found deleterious (S-shaped current-voltage characteristic), the results are encouraging when using graphene onto p-nc-Si:H and p-ncSi-O_x emitter. The best devices with graphene, complemented with optimized front DARC, show a short circuit current density increment of 1.4 mA/cm^2 with respect to our reference devices using AZO as TCE, which provides also antireflection effects. V_{oc} and FF are presently lower than the values of the reference cell, likely suffering from a still not optimized contact between graphene and underlying emitter material.

Regardless of the presently achieved performance, the observed, not so obvious, compatibility of Si-HJSCs with the proposed graphene implementation and transfer prove the high quality of transferred CVD-graphene over relevant area (up to 4 cm^2) and validate the feasibility of the graphene-over-device fabrication sequence, paving the way to graphene-integrated Si-HJSCs, free from plasma-based TCEs. The planned refinement of the graphene fabrication, transfer and handling procedures are all advancements that can also be applied to heterostructures based on other emerging two-dimensional materials.

Acknowledgments

This work was supported by the Italian Ministry of Economic Development in the framework of the Operating Agreement with ENEA for Research on the Electric System

References

[1] Yin Z, Zhu J, He Q, Cao X, Tan C, Chen H, Yan Q, Zhang H. Graphene-based materials for solar cell applications. Adv. Energy Mater 2013;4:1–19.

[2] Singh E, Nalwa H S. Graphene-Based Bulk-Heterojunction Solar Cells: A Review. J. Nanosci Nanotechnol. 2015;15(9):6237-78.

[3] Abdullah M, Hashim A. Review and assessment of photovoltaic performance of graphene/Si heterojunction solar cells. J. Mat. Sci. 2019;54(2):911–948.

[4] Di Bartolomeo A, Graphene Schottky diodes: An experimental review of the rectifying graphene/semiconductor heterojunction. Physics Reports. 2016;606:1-58.

[5] Li X, Zhu H. The graphene–semiconductor Schottky junction. Physics Today 2016;69(9):46-51

[6] Tu Z, Liu Z, Li Y, Yang F, Zhang L, Zhao Z, et al. Controllable growth of 1-7 layers of graphene by chemical vapour deposition. Carbon 2014;73:252-258.

[7] Chen Y, Gong X L, Gai J G. Progress and challenges in transfer of large-area graphene films. Adv. Sci. 2016;3:1500343.

[8] Chen X D, Liu Z B, Zheng C Y, Xing F, Yan X Q, Chen Y, et al. High-quality and efficient transfer of large-area graphene films onto different substrates. Carbon 2013;73:271278.

[9] Zhang Z, Du J, Zhang D, Sun H, Yin L, Ma L, et al. Rosin-enabled ultraclean and damage-free transfer of graphene for large-area flexible organic light-emitting diodes. Nat. Comm. 2017;8:14560.

[10] Rosli N N, Ibrahim M A, Ludin N A, Mat Teridi M A, Sopian K. A review of graphene based transparent conducting films for use in solar photovoltaic applications. Renewable and Sustainable Energy Reviews 2019;99:83–99.

[11] La Notte L, Bianco G V, Palma A L, Di Carlo A, Bruno G, Reale A. Sprayed organic photovoltaic cells and mini-modules based on chemical vapor deposited graphene as transparent conductive electrode. Carbon 2018;129:878-883.

[12] Masuko K, Shigematsu M, Hashiguchi T, Fujishima D, Kai M, Yoshimura N, et al. Achievement of more than 25% conversion efficiency with crystalline silicon heterojunction solar cell. IEEE J. Photovolt. 2014;4:1433–1435.

[13] Yoshikawa K, Kawasaki H, Yoshida W, Irie T, Konishi K, Nakano K, et al. Silicon heterojunction solar cell with interdigitated back contacts for a photoconversion efficiency over 26%. Nat. Energy 2017;2:17032.

[14]Park H, Chang S, Zhou X, Kong J, Palacios T, Gradecak S. Flexible graphene electrode-based organic photovoltaics with record-high efficiency. Nano Lett. 2014;14:5148-5154.

[15] Liu Z, You P, Liu S, Yan F. Neutral-color semitransparent organic solar cells with all-graphene electrodes. ACS Nano 2015;9:12026-12034.

[16] Song Y, Chang S, Gradecak S, Kong J. Visibly-transparent organic solar cells on flexible substrates with all-graphene electrodes. Adv.Energy Mater. 2016;6:1600847

[17] Mercaldo L V, Bobeico E, Usatii I, Della Noce M, Lancellotti L, Serenelli L, et al. Potentials of mixed-phase doped layers in p-type Si heterojunction solar cells with ZnO:Al. Solar Energy Materials and Solar Cells 2017;169:113–121.

[18] Della Noce M, Bobeico E, Lancellotti L, Mercaldo L V, Usatii I, Delli Veneri P. P-type SiOx front emitters for Si heterojunction solar cells. AIP Conference Proceedings 2019;2147:040003.

[19] Mercaldo L V, Usatii I, Delli Veneri P. Advances in thin-film Si solar cells by means of SiOx alloys. Energies 2016; 9:218.

[20] Baikie I D, Estrup P J. Low cost PC based scanning Kelvin probe". Review of Scientific Instruments 1998; 69(11):3902-3907.

[21] Lancellotti L, Bobeico E, Della Noce M, Delli Veneri P, Matacena I. Work Function Determination of Transparent Contact for a:Si/c-Si Heterojunction Solar Cells. Proceedings - 2018 IEEE International Conference on Environment and Electrical Engineering and 2018 IEEE Industrial and Commercial Power Systems Europe, EEEIC/I and CPS Europe 2018, art. no. 8493739. http://ieeexplore.ieee.org/xpl/mostRecentIssue.jsp?punumber=8476917 ISBN: 978-153865185-8. doi: 10.1109/EEEIC.2018.8493739.

[22] Nie S, Wu W, Xing S, Yu Q, Bao J, Pe S, et al. Growth from below: bilayer graphene on copper by chemical vapor deposition. New Journal of Physics 2012;14:093028.

[23] Liu J, Huang Z, Lai F, Lin L, Xu Y, Zuo C, et al. Controllable Growth of the Graphene from Millimeter-Sized Monolayer to Multilayer on Cu by Chemical Vapor Deposition. Nanoscale Research Letters 2015;10:455.

[24] Chen J J, Meng J, Yu D P, Liao Z M. Fabrication and Electrical Properties of Stacked Graphene Monolayers. Scientific Reports 2014;4:5065.

[25] Uemura K, Ikuta T, Maehashi K. Turbostratic stacked CVD graphene for high-performance devices. Japanese Journal of Applied Physics 2018;57(3):030311.

[26] Bivour M, Sebastian Schröer S, Hermle M. Numerical analysis of electrical TCO/a-Si:H(p)contact properties for silicon heterojounction solar cells. Energy Procedia 2013;38:658–669.

[27] Luongo G, Di Bartolomeo A, Giubileo F, Chavarin C A, Wenger C. Electronic properties of graphene/p-silicon Schottky junction. J. Phys. D: Appl. Phys. 2018;51:255305.

[28] Lancellotti L, Polichetti T, Ricciardella F, Tari O, Gnanapragasam S, Daliento S, et al. Graphene applications in Schottky barrier solar cells.Thin Solid Films 2012;522:390-394.

[29] https://www.thinfilmcenter.com.

[30] Lancellotti L, Bobeico E, Capasso A, Lago E, Delli Veneri P, Leoni E, et al. Combined effect of double antireflection coating and reversible molecular doping on performance of few-layer graphene/n-silicon Schottky barrier solar cells. Solar Energy 2016;127:198-205.

[31] Lancellotti L, Bobeico E, Castaldo A, Delli Veneri P, Lago E, Lisi N. Effects of different graphene dopants on double antireflection coatings/graphene/n-silicon heterojunction solar cells. Thin Solid films (2018);646:21-27.

[32] Richter A, Smirnov V, Lambertz A, Nomoto K, Welter K, Ding K. Versatility of doped nanocrystalline silicon oxide for applications in silicon thin-film and heterojunction solar cells. Solar Energy Materials and Solar Cells 2018;174:196–201.

[33] Seif J P, Descoeudres A, Nogay G, Hänni S, Martin de Nicolas S, Holm N. Strategies for Doped Nanocrystalline Silicon Integration in Silicon Heterojunction Solar Cells. IEEE Journal of Photovoltaics 2016;6(5):1132-1140.

[34] Mazzarella L, Kirner S, Stannowski B, Korte L, Rech B, Schlatmann R. P-type microcrystalline silicon oxide emitter for silicon heterojunction solar cells allowing current densities above 40 mA/cm^2. Appl. Phys. Lett. 2015;106:023902.

[35] Demaurex B, De Wolf S, Descoeudres A, Holman Z C, Ballif C. Damage at hydrogenated amorphous/crystalline silicon interfaces by indium tin oxide overlayer sputtering. Appl. Phys. Lett. 2012;101:171604.

[36] Demaurex B, Seif J P, Smit S, Macco B, Kessels W M M, Geissbühler J, et al. Atomic-layer-deposited transparent electrodes for silicon heterojunction solar cells. IEEE J. Photovolt. 2014;4(6):1387–1396.

[37] Macco B, Deligiannis D, Smit, van Swaaij R A C M M, Zeman M, Kessels W M M. Influence of transparent conductive oxides on passivation of a-Si:H/c-Si heterojunctions as studied by atomic layer deposited Al doped ZnO. Semicond. Sci. Technol. 2014;29:122001.

[38] Rößler R, Leendertz C, Korte L, Mingirulli N, Rech B. Impact of the transparent conductive oxide work function on injection-dependent a-Si:H/c-Si band bending and solar cell parameters. J. Appl. Phys. 2013;113:144513.
[39] Tomasi A, Sahli F, Seif J P, Fanni L, Martin de Nicolas Agut S, Geissbühler J, et al. Transparent electrodes in silicon heterojunction solar cells: influence on contact passivation. IEEE J. Photovolt. 2016;6:17–27.
[40] Demaurex B, Seif J P, Smit S, Macco B, Kessels W M M, Geissbühler J, et al. Atomic-layer-deposited transparent electrodes for silicon heterojunction solar cells. IEEE J. Photovolt. 2014;4:1387–1396.
[41] Li Y, Chen Z. XH/π (X = C, Si) Interactions in Graphene and Silicene: Weak in Strength, Strong in Tuning Band Structures,.J. Phys. Chem. Lett. 2013;4:269−275.
[42] Khomyakov P A, Giovannetti G, Rusu P C, Brocks G, van den Brink J, Kelly P J. First-principles study of the interaction and charge transfer between graphene and metals. Physical Review B 2009;79:195425.
[43] Song S M, Park J K, Sul O J, Cho B J. Determination of Work Function of Graphene under a Metal Electrode and Its Role in Contact Resistance. Nano Lett. 2012;12:3887−3892.

LIST OF FIGURE CAPTIONS

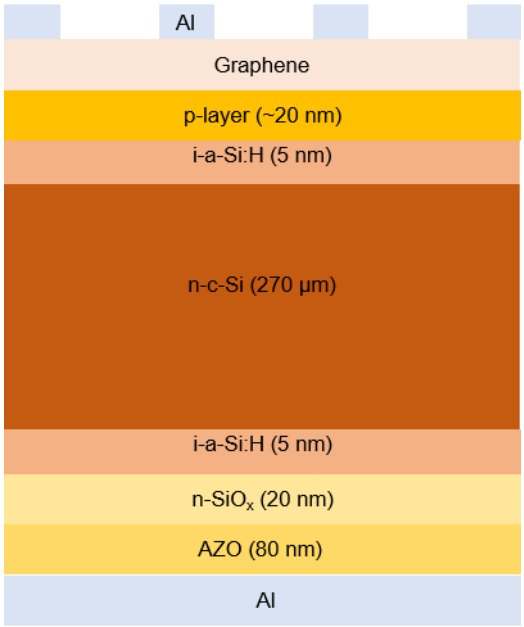

Fig. 1: Scheme of the graphene-integrated Si-HJSC investigated in this work.

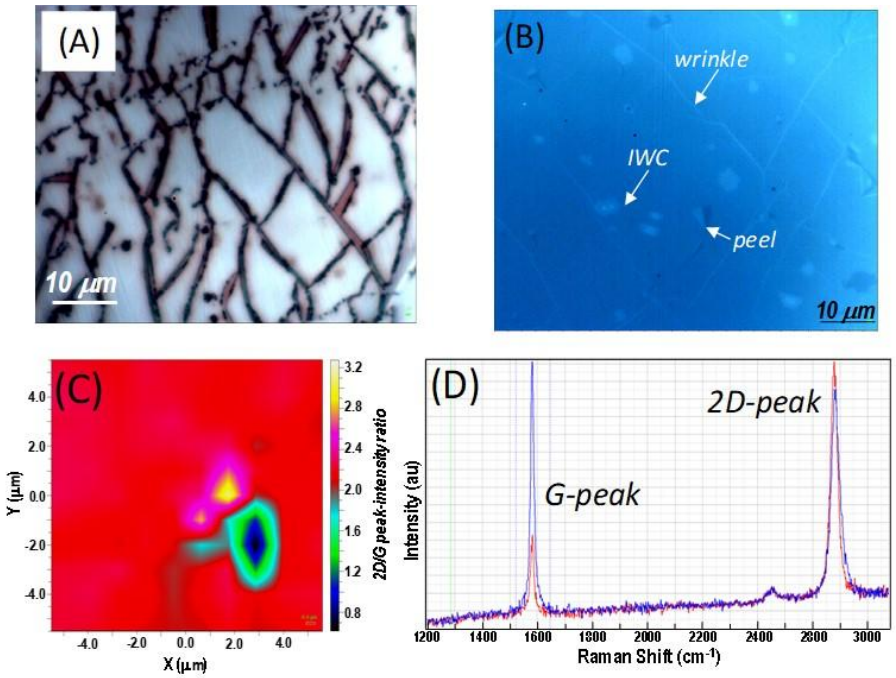

Fig. 2: Optical imaging (A,B) and Raman spectroscopy (C,D) investigation of single layer graphene: optical images of graphene/Cu after selective oxidation of the copper foil (A) and of graphene transferred on Corning glass (B); color scale map based on the 2D/G Raman peak intensity ratio, with red for monolayer and blue for bilayer (C); Raman spectra acquired within the monolayer (red) and bilayer (blue) regions (D).

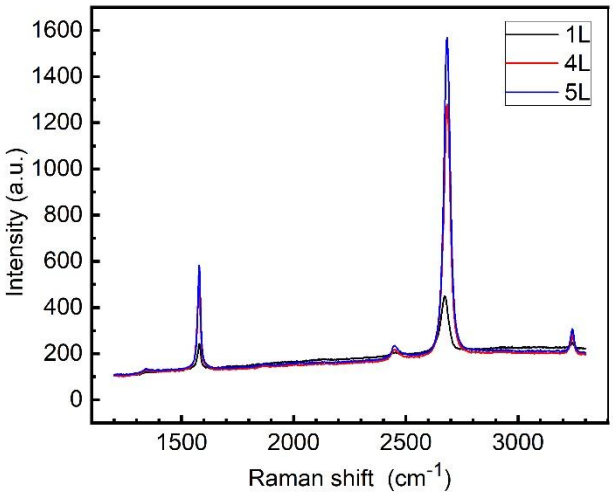

Fig. 3: Raman spectra of 1L-, 4L-, and 5L-graphene foils after layer-by-layer transfer onto a solar cell.

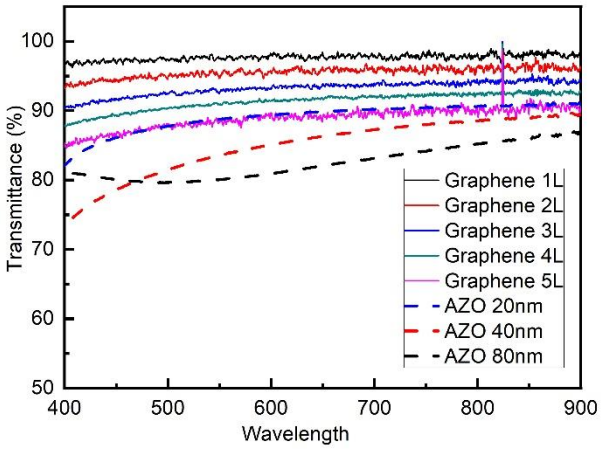

Fig. 4: Transmittance spectra of graphene films with different nL (solid lines) and 20, 40, and 80 nm thick AZO layers (dashed lines), all on glass substrates.

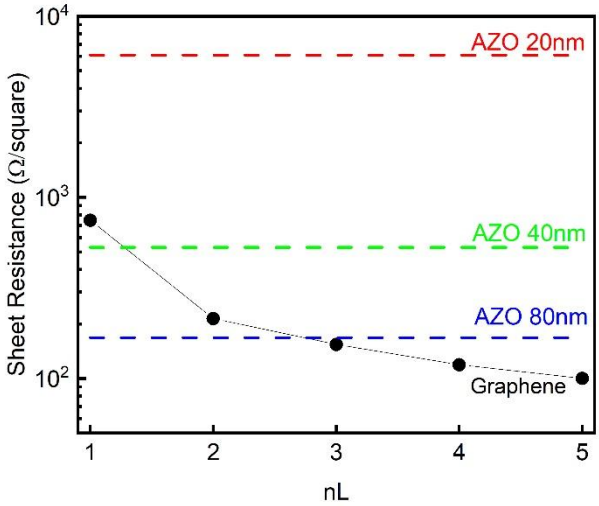

Fig. 5: Sheet resistance of graphene films with different nL (dots) and of 20, 40, and 80 nm thick AZO layers (dashed lines).

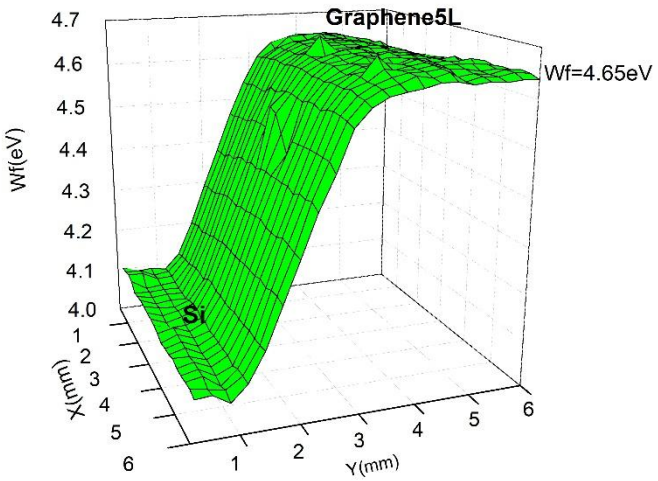

Fig. 6: WF map of a 5L graphene stack transferred on n-type Si wafer.

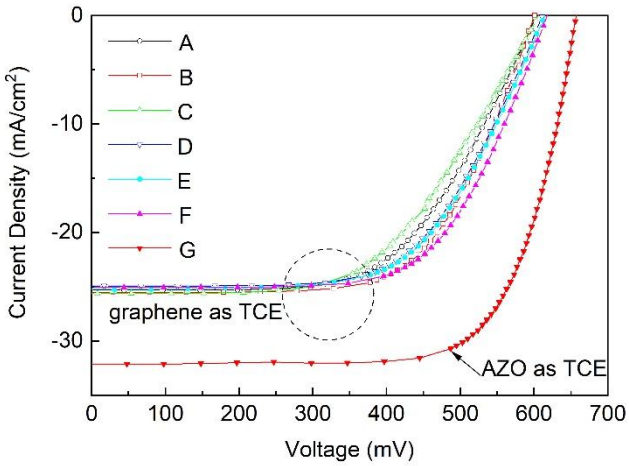

Fig. 7: Illuminated J(V) curves of 1cm^2 solar cells with p-nc-Si:H emitter with graphene (4L and 5L) or 80 nm thick AZO as TCE.

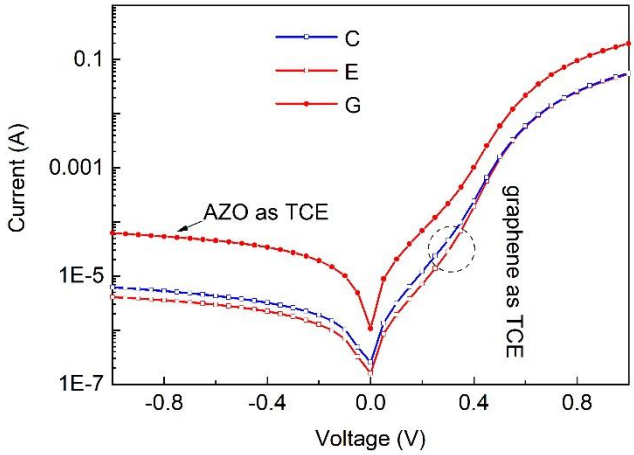

Fig. 8: Dark I-V characteristics of two representative solar cells with graphene compared with the reference cell with AZO.

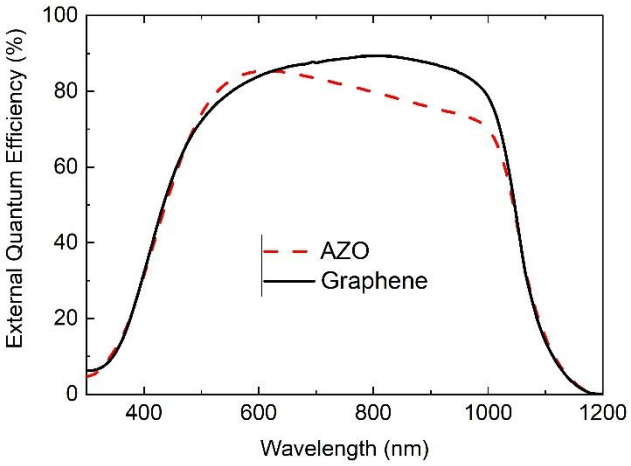

Fig. 9: EQEs of a graphene integrating solar cell with DARC and of the standard cell with AZO.

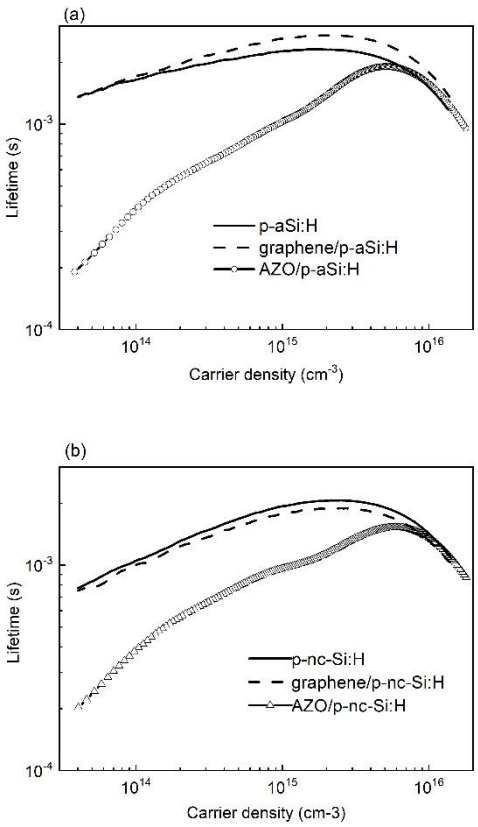

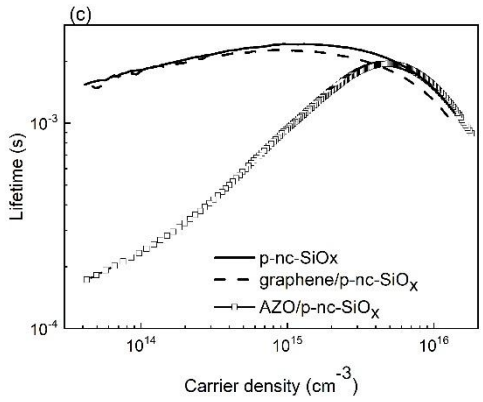

Fig. 10: Effective lifetime of solar cell precursors at various stages during front side fabrication prior to metallization. The samples are composed of the different front layer/layers indicated in the legends over the i-a-Si:H/n-c-Si/ i-a-Si:H/n-nc-SiOx:H/AZO stack.

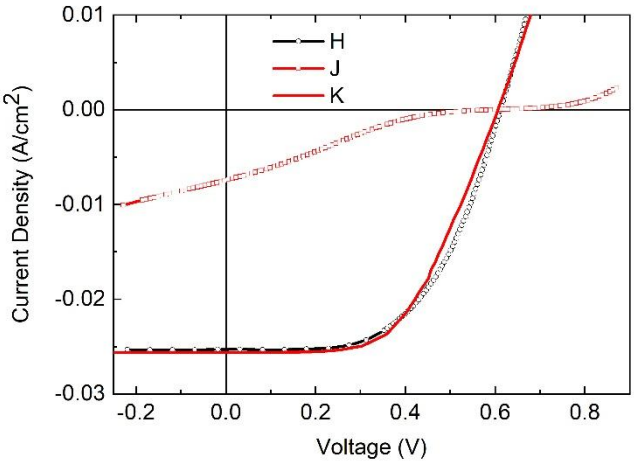

Fig. 11: Illuminated J(V) curves of representative 4 cm^2 Si HJSCs integrating 5L graphene as front TCE over different emitters.

LIST OF TABLES CAPTIONS

Front TCE	Cell	V_{oc}(mV)	J_{sc}(mA/cm^2)	FF(%)	Eff(%)
4L graphene	A	603	25.3	58.9	8.98
	B	601	25.5	64.0	9.81
	C	606	25.6	55.4	8.61
5L graphene	D	612	24.9	61.5	9.38
	E	615	25.3	61.1	9.48
	F	618	25.1	64.2	9.95
80 nm AZO	G	657	32.1	72.1	15.21

Table I: Photovoltaic parameters calculated from the curves reported in Fig. 7.

Emitter	V_{oc}(mV)	J_{sc}(mA/cm^2)	FF(%)	Eff(%)
p-nc-SiO_x	612	25.3	55.8	8.65
p-aSi:H	599	7.5	20	0.89
p-nc-Si:H	607	25.5	55.3	8.56

Table II: Photovoltaic parameters calculated from the curves reported in Fig. 11.